Determining the internal temperature of an optically levitated nanoparticle in vacuum by doped-Er^{3+}-ion luminescence

Baobao Zhang,[1] Xiaojun Guo,[1] Xudong Yu,[2] Yanzhen Xiao,[1] Zhengkun Fu,[1,*] Zhenglong Zhang,[1,†] and Hairong Zheng[1]
[1]*School of Physics and Information Technology, Shaanxi Normal University, Xi'an 710119, China*
[2]*State Key Laboratory of Quantum Optics and Quantum Optics Devices, Shanxi University, Taiyuan 030006, China*

(Received 8 February 2023; revised 29 June 2023; accepted 23 August 2023; published 7 September 2023)

In recent years, optically levitated systems have emerged as an important platform for conducting fundamental physics studies and precision measurements. The internal temperature of the levitated nanoparticles plays a critical role in determining the measuring sensitivity and decoherence of the system. In this study, we perform experiments on the internal temperature of a rare-earth-doped nanoparticle α-$NaYF_4$:Yb^{3+}/Er^{3+} levitated in an intermediate vacuum. To determine the internal temperature of the nanoparticle, we measure the luminescence intensity ratio of the thermally coupled levels of the doped Er^{3+} ions. Our results show that the internal temperature of the optically levitated nanoparticle increases as the air pressure decreases and that there is a coupling between the internal temperature and center-of-mass motion of the nanoparticle levitated in vacuum. We also find a correlation between the slow rise in internal temperature and the abrupt loss of the levitated nanoparticle, which can be used to guide stabilization of the optical trap.

DOI: 10.1103/PhysRevA.108.033503

I. INTRODUCTION

Optically levitated optomechanical systems, which operate at room temperature and in an isolated environment, offer immense potential for applications in fields such as quantum physics, materials science, nonequilibrium dynamics, and ultrasensitive sensing [1–3]. The precise measurement and control of particle dynamics are essential for these systems. However, the high internal temperatures pose a significant challenge as they can limit the force sensitivity or coherence of macroscopic quantum states and even result in trapping instability [4,5].

Several internal temperature measurement methods have been proposed for levitated nanoparticles, including analyzing the center-of-mass (COM) motion [6,7], displacement sensing [8], nitrogen vacancy thermometry [9–11], and luminescent thermometry by Yb^{3+}:YLF nanocrystals [12]. Among these methods, luminescence thermometry based on nanoparticles doped with rare earths stands out due to its remarkable features [13]. It exhibits high-temperature sensitivity, a wide temperature range, and noninvasive and noncontact measurement capability, which make it ideal for nanoscale temperature analysis [14,15]. The luminescence properties such as luminescence intensity, lifetime, peak shift, and spectral broadening of rare-earth-doped nanoparticles can be effectively utilized for thermometry [16]. Notably, luminescence intensity ratio thermometry has gained widespread adoption due to its reliability and simplicity.

Furthermore, the synthesis of the host matrix $NaYF_4$ can be precisely controlled to obtain nanoparticles with sizes suitable for single-beam optical trapping [17]. Its high refractive index and low optical absorption are also beneficial for optical levitation experiments [18,19]. Another advantage is the efficient upconversion luminescence of the codoped host matrix material $NaYF_4$ due to the large absorption cross-section Yb^{3+} ions and resonance energy transfer properties of Yb^{3+} to Er^{3+} ions [20]. In addition, rare-earth-doped nanoparticles can be cooled with anti-Stokes luminescence, giving them the potential to levitate in high vacuum with excellent thermal control ability [12,21]. Therefore, rare-earth-doped nanoparticles with upconversion luminescence are promising to be employed to monitor and control the internal temperature of levitation systems, notably for nonequilibrium dynamics experiments [22].

This study investigates the optical levitation and temperature sensing of rare-earth-doped nanoparticles $NaYF_4$:Yb^{3+}/Er^{3+} in an intermediate vacuum. The internal temperature of the nanoparticles can be determined by analyzing their upconversion spectra at different air pressures. The coupling between the internal temperature and the COM temperature has been observed by measuring the COM motion of the nanoparticles. Notably, it has been observed that the internal temperature of levitated nanoparticles gradually increases before being abruptly lost from the optical trap. These findings suggest that the rare-earth-doped nanoparticles offer a convenient and reliable temperature-sensing capability, which is interesting for nonequilibrium physics investigations.

II. EXPERIMENTAL SETUP

The experimental setup is shown in Fig. 1(a). To trap a nanoparticle in the vacuum chamber, we utilize a continuous wave laser (Laser Quantum OPUS, $\lambda = 1064$ nm) with a power of 150 mW, which is focused through a high numerical

*zkfu@snnu.edu.cn
†zlzhang@snnu.edu.cn

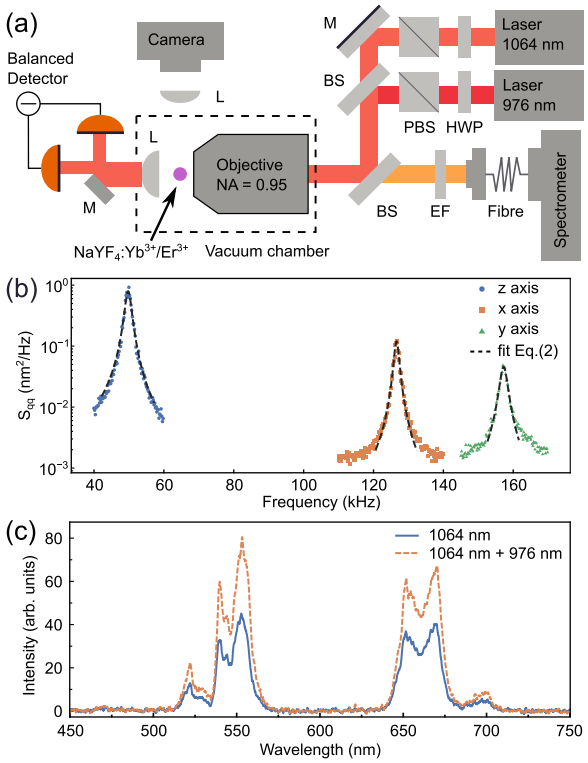

FIG. 1. (a) Schematic diagram of the setup for a levitated nanoparticle in vacuum (M, mirror; DM, dichroic mirror; BS, beam splitter; PBS, polarizing beam splitter; HWP, half-wave plate; EF, edge filter; L, lens). (b) The typical PSD of a levitated nanoparticle at 5 mbar. (c) Upconversion spectra of a levitated nanoparticle in vacuum under 1064-nm laser excitation and 1064- and 976-nm laser coexcitation.

aperture objective (Nikon, NA = 0.95). To excite or heat the levitated nanoparticles, a fiber laser (Connet Laser VLSS, $\lambda = 976$ nm) with variable power is employed. The nanoparticles used in the experiments are $NaYF_4$:20%Yb^{3+}/2%Er^{3+} nanocrystals with the cubic crystal phase synthesized by the hydrothermal method, and the Yb^{3+}/Er^{3+} dopants enable efficient upconversion luminescence. The size is determined by scanning electron microscopy images to be 153 ± 26 nm, as detailed in Appendix A. The motion of a levitated nanoparticle along the x, y, and z axes is measured with the interferometric detection scheme [23] by collecting scattered light in the forward direction with an aspheric lens (NA = 0.6). The luminescence of the levitated nanoparticle is collected in the backward direction with the same objective and measured with a spectrometer (Princeton Instruments, SP2750). Therefore, the spectra and COM motion of nanoparticles levitated in vacuum can be observed simultaneously.

We set the z axis of particle motion in the longitudinal direction, and x and y are transverse, where x is parallel to the polarization direction of the 1064-nm laser and y is perpendicular. The COM motion of the levitated nanoparticle in an optical trap in each direction (x, y, and z axes) is approximated by a damped harmonic oscillator model [24]:

$$m\ddot{q}(t) + m\Gamma_0\dot{q}(t) + m\Omega_0^2 q(t) = F_{\mathrm{fluct}}(t), \tag{1}$$

where m is the mass of the nanoparticle, q is the position, Γ_0 is the damping rate, Ω_0 is the natural oscillation frequency, and F_{fluct} is the random fluctuating force generated by the collision of air molecules with the nanoparticle.

The power spectral density (PSD) of the position q is given by [25]

$$\hat{S}_{qq}(\Omega) = \frac{2k_B T_{\mathrm{com}}}{m} \frac{\Gamma_0}{\left(\Omega^2 - \Omega_0^2\right)^2 + \Gamma_0^2\Omega^2}. \tag{2}$$

Here, k_B is Boltzmann constant, T_{com} is the COM temperature of the nanoparticle. The signal from the balance detector is converted into the displacement of a levitated nanoparticle according to the calibration factor determined by the equipartition theorem [24]. The typical PSD obtained from a levitated $NaYF_4:Yb^{3+}/Er^{3+}$ nanoparticle is shown in Fig. 1(b). The oscillation frequencies $\Omega_0 = \sqrt{k_{\mathrm{trap}}/m}$ are related to the trap stiffness $k_{\mathrm{trap}} = \alpha E_0^2/w^2$, where α is particle polarizability, E_0 is the electric field intensity, and w is the beam waist radius [26]. Typical natural oscillation frequencies $\Omega_0/2\pi$ are 126.6, 157.2, and 49.8 kHz in each direction (x, y, and z, respectively).

As shown in Fig. 1(c), the upconversion emission spectra of rare earth-doped nanoparticles $NaYF_4:Yb^{3+}/Er^{3+}$ are obtained under 1064-nm laser excitation and 1064- and 976-nm laser coexcitation. The upconversion emission of nanoparticles is attributed to the energy transfer process from doped Yb^{3+} ions to Er^{3+} ions. The energy mismatch between the excitation wavelength of 1064 nm and the energy level of Yb^{3+} can be compensated by the phonon assist in the host lattice [27]. Since the absorption cross section of doped Yb^{3+} ions at the resonance wavelength of 976 nm is larger than that of 1064 nm, more efficient upconversion luminescence is produced under the excitation of the 976-nm laser [28]. The existence of nonradiation phonon relaxation in the upconversion luminescence process also results in heat generation in nanoparticles, which we believe is the primary cause of the rise in internal temperature of the nanoparticles in the optical trap.

III. INTERNAL TEMPERATURE

Since the luminescence of rare-earth-doped nanoparticles depends remarkably on the temperature, the internal temperature of a $NaYF_4:Yb^{3+}/Er^{3+}$ nanoparticle levitated in vacuum can be easily obtained from upconversion spectra. The basic principle is that the population of the thermally coupled energy levels of rare-earth-doped nanoparticles follows the Boltzmann distribution, and its emission intensity is proportional to the population [15].

As shown in Fig. 2(a), the energy levels $^2H_{11/2}$ and $^4S_{3/2}$ of the doped Er^{3+} ions are thermally coupled, which are frequently employed for luminescence intensity ratio thermometry [13]. The green emission spectra of levitated nanoparticles doped with Er^{3+} ions at different air pressures are collected, and the spectra are smoothed and normalized at 540 nm [Fig. 2(b)]. The green emission bands ($\lambda 1$-$\lambda 2$) and ($\lambda 2$-$\lambda 3$) are attributed to the energy level transition of Er^{3+} ions from the excited states $^2H_{11/2}$ and $^4S_{3/2}$ to the ground state $^4I_{15/2}$, respectively [29,30]. The specific values of $\lambda 1$

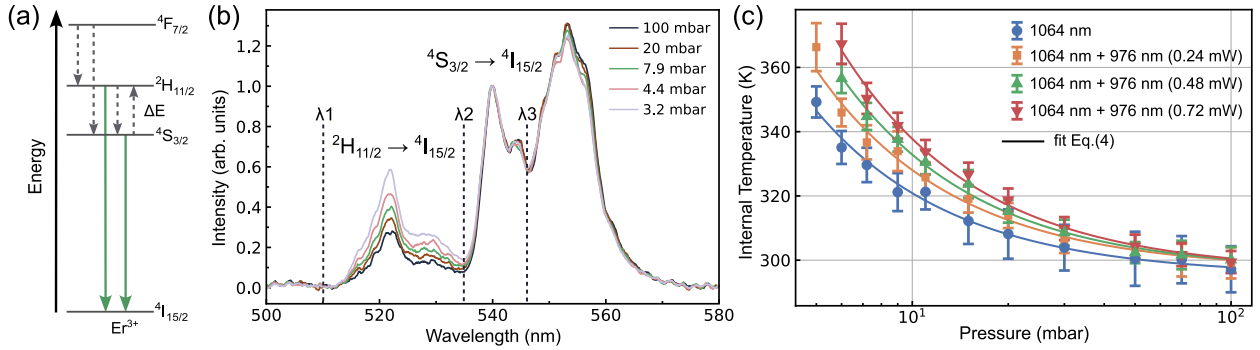

FIG. 2. (a) Schematic diagram of the transition of thermal coupling energy levels of Er^{3+} ions. (b) Luminescence spectra of the $NaYF_4$:Yb^{3+}/Er^{3+} nanoparticles at different air pressures. (c) The internal temperature of the levitated nanoparticle trapped by the 1064-nm laser and irradiation by the 976-nm laser at different air pressures. The solid lines are fits to the data according to Eq. (4).

(515 nm), λ2 (535 nm), and λ3 (546 nm) follow a common convention used in other luminescence thermometry studies [31,32]. It is found that the integrated intensity of the green emission band (λ1-λ2) increased significantly with decreasing air pressure, which indicates a higher internal temperature of the nanoparticles. The luminescence intensity ratio of the thermally coupled energy levels is described by the following equation [33]:

$$\ln(\mathcal{R}_{\rm lum}) = \ln\left(\frac{I_2}{I_1}\right) = -\frac{\Delta E}{k_{\rm B}}\frac{1}{T_{\rm int}} + C, \tag{3}$$

where $T_{\rm int}$ is the internal temperature, and I_2 and I_1 are the integral luminescence intensity of the emission bands (λ1-λ2) and (λ2-λ3), respectively. ΔE is the gap of thermally coupled energy levels, and the constant C is related to the emission rates and the integration boundary in the spectrum. Therefore, the internal temperature of the nanoparticles can be obtained from the spectra of Er^{3+} ions. The parameters $\Delta E = 743(5)$ cm^{-1} and constant $C = 2.73(2)$ of the luminescence thermometer are calibrated by the heating platform, as detailed in Appendix C.

As shown in Fig. 2(c), the dependence of the internal temperature of a levitated nanoparticle on the air pressure under 1064-nm laser excitation or 1064- and 976-nm laser coexcitation, where the internal temperature is calculated using Eq. (3) with the calibrated parameters. The error bars are derived from the uncertainty of the thermometer calibration coefficient and the standard deviation of the data from repeated measurements. Since the experimental particles are nanoscale and have good thermal conductivity, it is expected that the internal temperature distribution is uniform.

The heating of the levitated nanoparticles is due to the absorption of the laser, while the heat dissipation is attributed to the collision of air molecules, black-body radiation, and the radiative relaxation from the energy level transitions [12,34]. In order to simplify the model, the heat dissipation from black-body radiation and the luminescence of nanoparticles is neglected, as detailed in Appendix D. When the heating and dissipation of the system reaches a balanced state, the internal temperature of the levitated nanoparticles is given as [11]

$$T_{\rm int} = T_0 + C_{\rm heat}/p_{\rm air}, \tag{4}$$

where the heating coefficient $C_{\rm heat}$ is

$$C_{\rm heat} = \frac{2T_0 N I_{\rm las}\sigma_{\rm abs}}{\alpha_g \pi r^2 \bar{v}}\frac{\gamma - 1}{\gamma + 1}. \tag{5}$$

$I_{\rm las}$ is the power density of the laser, N is the number of Yb^{3+} ions in a single nanoparticle, $\sigma_{\rm abs}$ is the absorption cross section of Yb^{3+} ions, $\alpha_g \approx 1$ is the thermal accommodation coefficient, r is the radius of the nanoparticle, $\bar{v} \approx 500$ ms^{-1} is the mean speed of air molecules, $p_{\rm air}$ is the air pressure, $\gamma = 7/5$ is the ratio of specific heat for air, and $T_0 = 293$ K is the environmental temperature.

The fitting results show that the absorption cross sections $\sigma_{\rm abs}$ of Yb^{3+} at 1064 and 976 nm are $1.06(26) \times 10^{-22}$ and $1.10(20) \times 10^{-20}$ cm^2, respectively. The results take into account the uncertainty in nanoparticle size and thermal accommodation coefficient, which are consistent with the average of different particle measurements, as detailed in Appendix D. In this study, a simplified model with large parameter uncertainties is employed. Nonetheless, the absorption cross section of Yb^{3+} ions in a single nanoparticle is successfully measured with the optical levitation system. Notably, the obtained results exhibit comparability with previous reports on the absorption cross section of Yb^{3+} ions [28,35].

In a high vacuum, optically levitated nanoparticles will only emit black-body radiation for heat dissipation. However, the doping concentration of nanoparticles cannot be reduced down to the level where the luminescence is detectable and the absorption is low enough to achieve equilibrium with the black-body radiation. Therefore, optical cooling solids based on anti-Stokes fluorescence under suitable wavelength excitation may be required to achieve high vacuum levitation of rare-earth-doped nanoparticles with upconversion luminescence.

IV. COM TEMPERATURE

Due to interaction between the levitated nanoparticles and the air molecules in the surrounding environment, the COM motion of a levitated nanoparticle will be affected by its internal temperature [6]. To investigate the coupling between the internal temperature of the nanoparticle and its COM motion, the COM dynamics and upconversion spectra are measured simultaneously at different air pressures. The absolute internal temperature of the particle $T_{\rm int}$ can be deduced from the

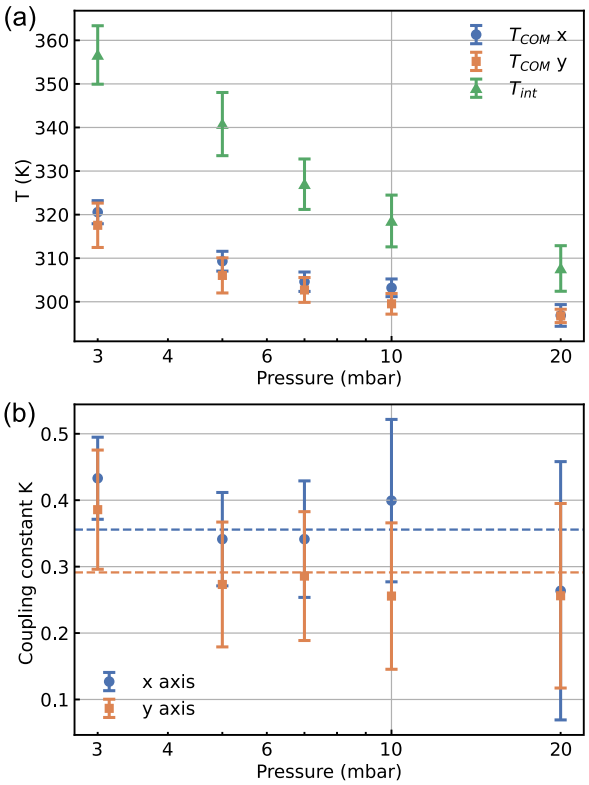

FIG. 3. (a) The COM temperature and internal temperature of a levitated nanoparticle trapped by a 1064-nm laser at different air pressures. (b) The coupling constant K between internal temperature and COM temperature of a levitated nanoparticle trapped by a 1064-nm laser at different air pressures.

upconversion spectrum, and the COM temperature T_{COM} of the nanoparticle can be resolved by fitting the PSD curve. As shown in Fig. 3(a), the COM temperature and the internal temperature of a levitated nanoparticle are both increasing with the air pressure decreasing, and the rise in COM temperature is less than the rise of the internal temperature.

In order to quantify the coupling between the internal temperature and the COM motion, the coefficient K is introduced [36]:

$$K = \frac{\Delta T_{\mathrm{COM}}}{\Delta T_{\mathrm{int}}} = \frac{T_{\mathrm{COM}} - T_0}{T_{\mathrm{int}} - T_0}. \tag{6}$$

The coefficient K is the ratio of the COM temperature rise to the internal temperature rise, while T_0 is the initial COM temperature and internal temperature. The coefficient K along the x and y axes at different air pressures is plotted in Fig. 3(b) and the averaged values of K are 0.36(6) and 0.29(5), respectively.

This result can be explained with the two-bath model that describes the coupling of the internal temperature of a levitated nanoparticle to its COM motion [6]. In the Knudsen regime, a levitated nanoparticle is heated above room temperature by absorbing laser. The impinging gas molecules collide with the hot nanoparticle in an inelastic way, and the emerging gas molecules are scattered by the nanoparticle with higher energy. These emerging gas molecules act as another thermal bath with a high effective emerging temperature that contributes to the COM motion of the levitated nanoparticle.

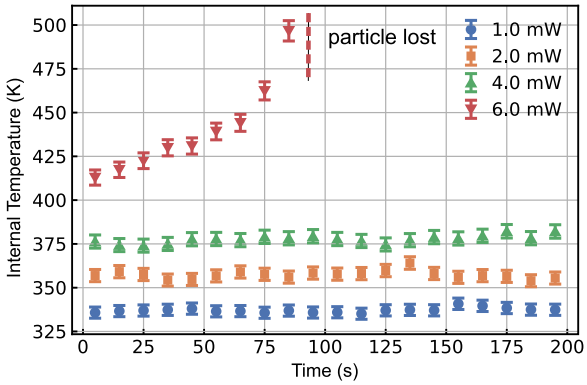

FIG. 4. The time-dependent internal temperature of a levitated nanoparticle under the radiation of different powers of a 976-nm laser at 20 mbar.

The thermal accommodation coefficient α_g represents the heat transfer rate by collision between air molecules and nanoparticles, and the relationship between K and α_g is $K = \pi/(\pi + 8)\alpha_g$, which is derived from the approximation of the two-bath model [6,36]. Therefore, the thermal accommodation coefficients α_g for the x and y axes are calculated as 1.26(21) and 1.03(17), respectively. This value is approximately the maximum accommodation coefficient $\alpha_g = 1$, which means that the air molecules collide with nanoparticles in a completely inelastic way, and also represents the maximum coupling between the internal temperature and the COM motion of a levitated nanoparticle. The value calculated from the two-bath model slightly exceeds the maximum value of 1, which is probably due to the desorption of ligand molecules from the levitated nanoparticle surface at high temperatures and thus increases the energy of the emerging gas molecules.

V. PARTICLE LOST

Similar to previous reports on nanodiamonds, $NaYF_4$:Yb^{3+}/Er^{3+} nanoparticles used in this experiment can also been stably levitated at air pressure from the atmosphere down to 10 mbar and generally escape from the trap between 1 to 10 mbar [9,34,36]. There are many hypotheses about the reasons for particle loss at decreased air pressure, including Kramer's escape [9], particle burning [37], temperature distribution inhomogeneity [38], and anisotropic overheating [36], but a clear understanding of the mechanisms is still lacking.

To further understand the escape of nanoparticles, we heat a levitated nanoparticle with the 976-nm laser and monitor its internal temperature to examine the stability of trapping. Due to the low spectral acquisition efficiency of the device, the temporal resolution of the temperature measurement is limited to 10 s. This time interval of measurement is much longer than the temperature rise of the nanoparticles due to laser absorption, so the initial rapid temperature rise process is not observed. In Fig. 4, we show the time-dependent internal temperature of a nanoparticle levitated by a 1064-nm laser in a vacuum at 20 mbar. The error bars are derived from the uncertainty of the thermometer calibration coefficient.

Under the excitation of 1, 2, and 4 mW of a 976-nm laser, the internal temperature of nanoparticles increases immediately and then remains stable. With the increase of the 976-nm laser power to 6 mW, a slow heating process lasting more than 80 s can be observed in addition to the initial rapid heating process. Moreover, when the internal temperature of the $NaYF_4$:Yb^{3+}/Er^{3+} nanoparticle exceeds 500 K, it is suddenly lost from the optical trap. More experimental data on the escape of levitated nanoparticles from optical traps are available in Appendix E. Although the specified parameters are different, both of them follow the same pattern of slowly increasing internal temperature before escaping. The experimental results also show that the 976-nm laser acts by heating the nanoparticles to increase their internal temperature, which causes them to escape from the optical trap. In the absence of the 976-nm laser, the same effect can be achieved by reducing the ambient air pressure to reduce thermal dissipation, which also increases the internal temperature of the nanoparticles.

It is noticed that there is a strong correlation between the slow increase of the internal temperature and the escape of nanoparticles from the optical trap. The high internal temperature not only affects the COM motion of $NaYF_4$:Yb^{3+}/Er^{3+} nanoparticles but also may trigger complex structural or morphological transformations, which have a negative impact on the stability of the trapping. However, more research is still needed to gain a comprehensive insight into the internal-temperature-related loss mechanisms. Although this study focuses on levitated rare-earth-doped nanoparticles, the results regarding nanoparticle escape from optical traps could be extended to other types of nanoparticles, such as nanodiamonds and SiO_2 nanospheres. It is worth noting that the heating effect of a laser on nanoparticles goes beyond the nonradiative relaxation from energy level transitions and includes the optical absorption of host material and impurity defects [7,34,37,39]. Therefore, different types of nanoparticles may also escape from the optical trap due to laser-induced heating effects leading to an increase in their internal temperature.

VI. CONCLUSION

In summary, we have observed the upconversion luminescence of rare-earth-doped nanoparticles $NaYF_4$:Yb^{3+}/Er^{3+} optically levitated in an intermediate vacuum. The internal temperature of a levitated nanoparticle can be calculated from thermally coupled energy level emission ratios, and the results indicate that a decrease in air pressure leads to an increase in internal temperature. The coupling between the internal temperature and the COM temperature of a levitated nanoparticle has also been examined experimentally. In addition, the escape of nanoparticles from the optical trap is found to be strongly linked to the increase in the internal temperature. Thus, the solid-state laser refrigeration based on anti-Stokes luminescence is a promising strategy to address the heating problem associated with optical trapping of $NaYF_4$:Yb^{3+}/Er^{3+} nanoparticles in high vacuum.

ACKNOWLEDGMENTS

This work has been supported by the National Natural Science Foundation of China (Grants No. 92050112, No. 92150110, No. 12074237, No. 12004233, No. 61975101, and No. U22A6005), the Natural Key R&D Program of China (Grants No. 2020YFA0211300 and No. 2021YFA1201500), the Fundamental Science Foundation of Shaanxi (Grant No. 22JSZ010), the Fundamental Research Funds for Central Universities (Grants No. GK202201012 and No. GK202308001), and the Program of State Key Laboratory of Quantum Optics and Quantum Optics Devices (Grant No. KF202003).

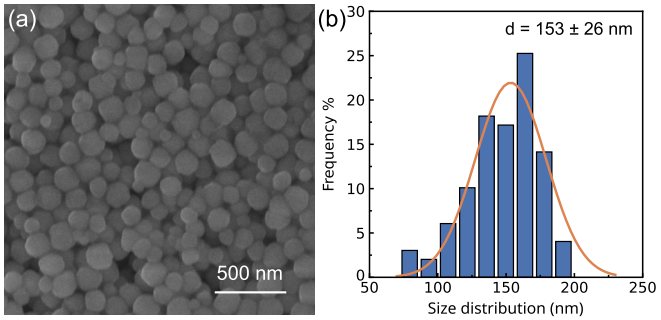

FIG. 5. (a) The SEM image of $NaYF_4$:Yb^{3+}/Er^{3+} nanoparticles. (b) Size distribution of $NaYF_4$:Yb^{3+}/Er^{3+} nanoparticles and the Gaussian fit curve.

APPENDIX A: MORPHOLOGY CHARACTERIZATIONS

As shown in Fig. 5, the morphology of nanoparticles is characterized by scanning electron microscopy (SEM).

APPENDIX B: NATURAL FREQUENCY OF COM MOTION

The relationship between the natural oscillation frequency of nanoparticles in the optical trap and the beam waist radius w is given below [26]:

$$\Omega_0 = \sqrt{\alpha E_0^2/m}/w. \tag{B1}$$

Therefore, the oscillation frequency is inversely proportional to the waist spot radius. The parameters of the focused laser spot are listed in Table I.

The mass m of a single nanoparticle is calculated based on the size of the nanoparticle and the uncertainty is estimated according to the error propagation formula. The size of the laser spot focused by the objective is measured using the razor blade method. The position where the laser intensity is reduced to $1/e^2$ is defined as the waist radius, which is 0.739(10) and 0.635(9) μm in the x and y axis directions, respectively, while the Rayleigh length z_0 is 1.385(27) μm. The experimentally measured COM motion frequency ratio of the levitated nanoparticle between the x, y, and z axes is 2.54:3.16:1. The different spot sizes along the x- and y-axis directions give rise to the variation in the resonant frequen-

TABLE I. The parameters of the focused laser spot.

Quantity	m (kg)	w_x (μm)	w_y (μm)	z_0 (μm)
Value	7.6×10^{-18}	0.739	0.635	1.385
Uncertainty	3.9×10^{-18}	0.010	0.009	0.027

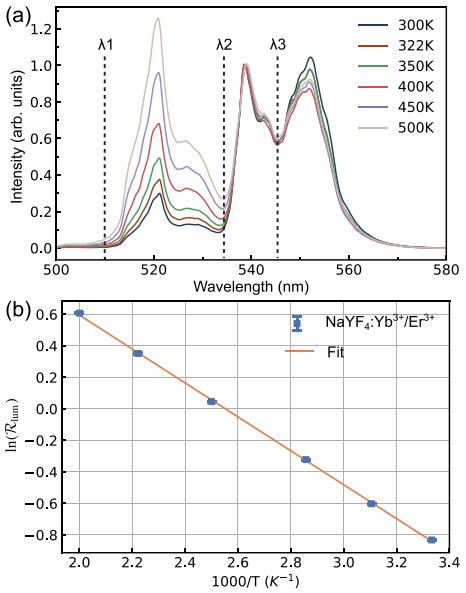

FIG. 6. (a) Emission spectra of Er^{3+} ions are measured on the thermal platform at different temperatures of 300–500 K. (b) Dependence of the emission intensity ratio [$\ln(\mathcal{R}_{\rm lum})$] of the Er^{3+} ions on the inverse of temperature (1000/T). The parameters of the luminescence thermometry can be obtained by fitting the data measured by the thermal platform.

cies of the nanoparticles. Compared with the x- and y-axis directions, the light field along the z-axis direction is less focused, resulting in a smaller optical trap stiffness along the z-axis direction. Therefore, the resonant frequencies of nanoparticles in the z-axis direction are significantly lower than those along the x- and y-axis directions [40].

APPENDIX C: LUMINESCENCE THERMOMETRY

To obtain the parameters in the luminescence thermometry, the luminescence intensity ratio of a single $NaYF_4$:Yb^{3+}/Er^{3+} nanoparticle is calibrated via a thermal platform. The sample is monodispersed on the wafer and keeps in good contact with the thermal platform, which is set at a temperature of 300–500 K. After the sample reaches thermal equilibrium with the thermal platform, the sample luminescence spectra are measured. In Fig. 6, the luminescence intensity ratios of the samples at different temperatures are calculated, and a linear fit is made to the inverse of the luminescence intensity ratio versus temperature [33,41]:

$$\mathcal{R}_{\rm lum} = \frac{\int_{\lambda_1}^{\lambda_2} I(\lambda)d\lambda}{\int_{\lambda_2}^{\lambda_3} I(\lambda)d\lambda} = \exp\left(-\frac{\Delta E}{k_{\rm B}T}\right) + B, \tag{C1}$$

$$\ln(\mathcal{R}_{\rm lum}) = -\frac{\Delta E}{1000 \times k_{\rm B}} \times \frac{1000}{T} + C. \tag{C2}$$

The results of the fit show that the slope of the line is $-1.07(1)$; therefore, ΔE is 743(5) $\rm cm^{-1}$ and the constant C is 2.73(2).

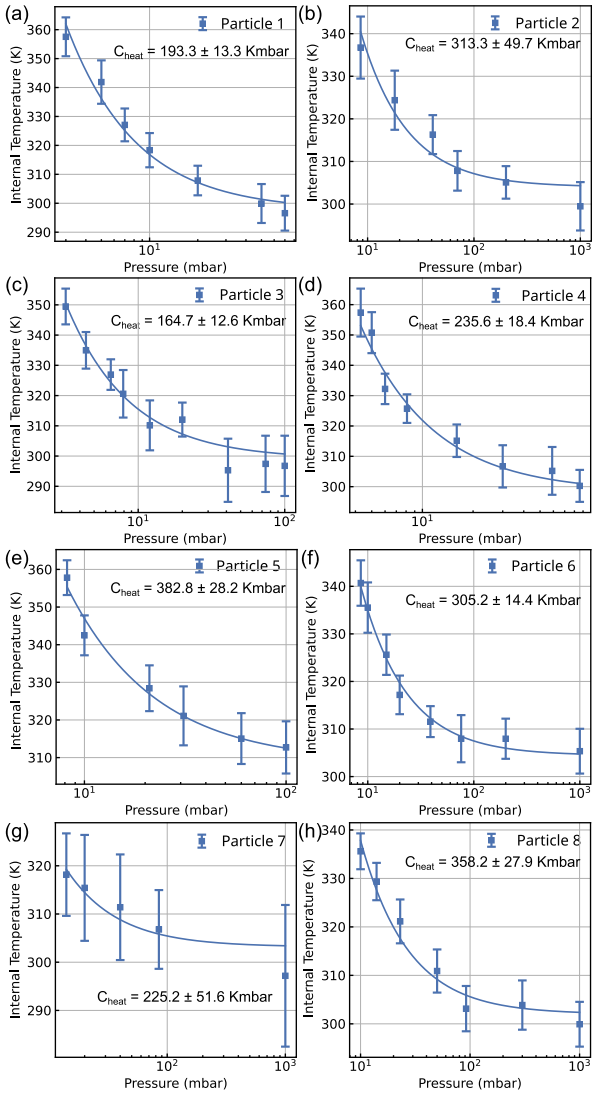

FIG. 7. (a)–(h) The dependence of the internal temperature of different rare-earth-doped nanoparticles on the air pressure under the excitation of a 1064-nm laser.

APPENDIX D: Internal Temperature

To derive the dependence of the internal temperature of a levitated nanoparticle on the air pressure, a gas collision thermal dissipation model is used here. The sensitizer Yb^{3+} ions have a larger absorption cross section relative to the matrix material as well as Er^{3+} ions [42], and it can be assumed that the absorption of rare-earth-doped nanoparticles is mainly from Yb^{3+} ions. Therefore, it is reasonable to assume that the absorbed power is linearly related to the number of Yb^{3+} ions in the nanoparticle. The laser power absorbed by a levitated nanoparticle can be expressed as [43]

$$P_{\rm abs} = N I_{\rm las} \sigma_{\rm abs}, \tag{D1}$$

where N is the number of Yb^{3+} ions in a single nanoparticle, $I_{\rm las}$ is the power density of the laser, and $\sigma_{\rm abs}$ is the absorption cross section of Yb^{3+} ions. The specific value of N is estimated by the size of the nanoparticles as well as the doping concentration of Yb^{3+} ions. First, the diameter d of

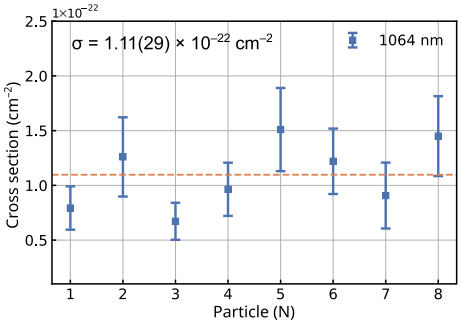

FIG. 8. The absorption cross sections at 1064 nm for Yb^{3+} ions of different nanoparticles. The error bars in the figure are derived from the standard deviation of the repeated measurements of the spectra, as well as the uncertainty of the nanoparticle size and the heat accommodation coefficient.

nanoparticles is determined as 153(26) nm, based on the characterization of SEM images, and their volume $V = \frac{4}{3}\pi(d/2)^3$ can be calculated. Then, the number N_{cell} of $NaYF_4$ unit cells is obtained from the ratio of the volume of nanoparticles to that of a single unit cell, which is $N_{\text{cell}} = V/a_c^3$. The typical lattice parameter for cubic $NaYF_4$ crystal is $a_c = 5.51$ Å [44]. Finally, the number of Yb^{3+} ions contained in a single nanoparticle, N, is obtained by considering the doping concentration (20%) of Yb^{3+} ions, which is $N = 2N_{\text{cell}} \times 20\% = \pi d^3/15a_c^3$.

The heat dissipation power of a levitated nanoparticle by the collision of air molecules is [11,34]

$$P_{\text{cond}} = \frac{\alpha_g}{2}\pi r^2 \bar{v} p_{\text{air}} \frac{\gamma+1}{\gamma-1}\left(\frac{T_{\text{int}}}{T_0} - 1\right), \tag{D2}$$

where α_g is the thermal accommodation coefficient, $r = d/2$ is the radius of the nanoparticle, $\bar{v}$ is the mean speed of air molecules, p_{air} is the air pressure, γ is the ratio of specific heat for air, T_{int} is the internal temperature of the nanoparticle, and T_0 is the environmental temperature.

The power dissipated by the nanoparticle to produce radiative relaxation luminescence by energy level transitions is [45]

$$P_{\text{em}} = \eta_q P_{\text{abs}} = \frac{W_{\text{r}}}{W_{\text{r}} + W_{\text{nr}}} P_{\text{abs}}, \tag{D3}$$

TABLE II. List of parameters for calculating the absorption cross section of Yb^{3+} ions.

Quantity	Value	Uncertainty
r	77 nm	13 nm
α_g	1.03	0.17
N	4.5×10^6	2.3×10^6
I_{las}	10^7 W/cm^2	—
T_0	293 K	—
$\bar{v}$	500 m/s	—
γ	7/5	—
a_c	5.51 Å	—
ΔE	743 cm^{-1}	5 cm^{-1}
C	2.73	0.02

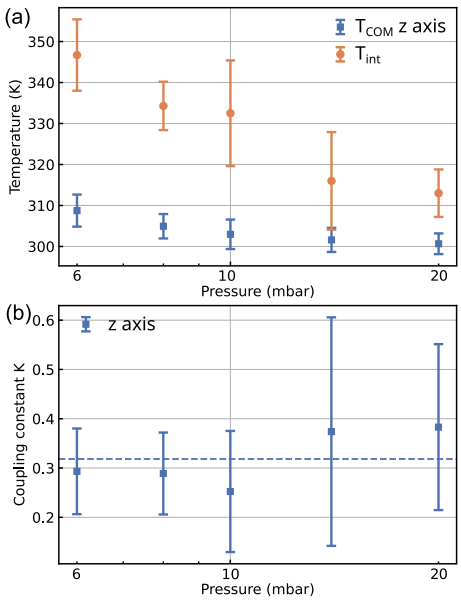

FIG. 9. (a) The internal temperature of a levitated nanoparticle and the COM temperature in the z axis direction. (b) Coupling constant K between the internal temperature of a levitated nanoparticle and the COM temperature in the z axis direction.

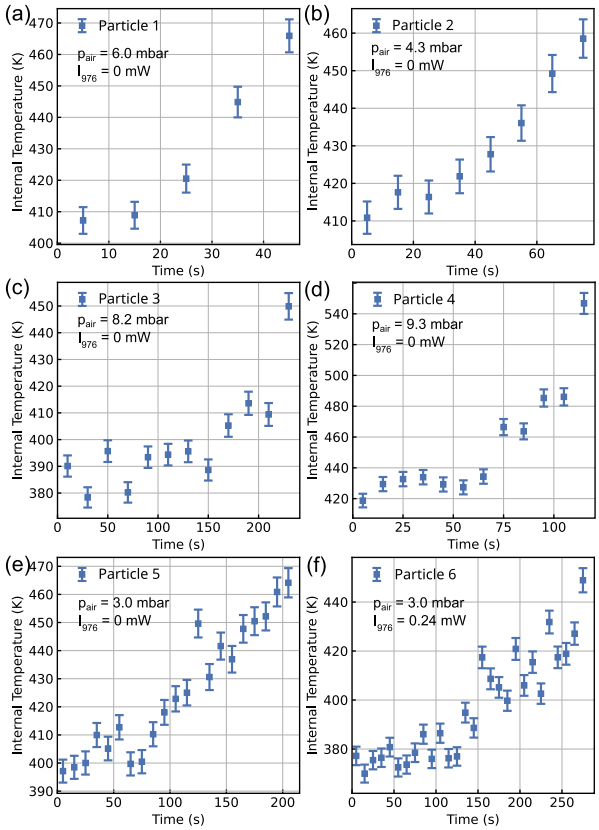

FIG. 10. (a)–(f) More examples of levitated nanoparticles escaping from optical traps. These levitated nanoparticles undergo a slow rise in their internal temperature before escaping from the optical traps at different air pressures, with or without the presence of a 976-nm laser.

η_q is the internal quantum yield of the nanoparticle, while W_r and W_{nr} are the radiative and nonradiative relaxation rates of the excited state, respectively. For typical $NaYF_4$:20%Yb^{3+}/2%Er^{3+} nanoparticles with cubic phase, the inner quantum yield is generally low and thus can be neglected [46]. In addition, the black-body radiation of the nanoparticles also can be negligible in the relative low-temperature range (<400 K). Therefore, when the system temperature is stable, the laser heating power of the nanoparticles is balanced with the air conduction power, i.e., $P_{abs} = P_{cond}$. As a result, according to Eqs. (4) and (5), the absorption cross section σ_{abs} can be expressed as

$$\sigma_{abs} = \frac{\alpha_g \pi r^2 \bar{v}}{2T_0 N I_{las}} \frac{\gamma+1}{\gamma-1} C_{heat} = \frac{15\alpha_g a_c^3 \bar{v}}{16T_0 r I_{las}} \frac{\gamma+1}{\gamma-1} C_{heat}. \quad \text{(D4)}$$

In Figs. 7 and 8, the heating coefficient C_{heat} can be obtained by fitting the experimental data, and thus the absorption cross section of Yb^{3+} ions can be calculated.

The parameters used to calculate the absorption cross section of Yb^{3+} ions are listed. The radius r of nanoparticles is obtained from SEM characterization and the uncertainty is derived from the statistical results of multiple nanoparticles. The thermal accommodation coefficients α_g are derived from the experimental values for nanoparticles in Fig. 3 of the manuscript. The number N of Yb^{3+} ions in a single nanoparticle is calculated based on the size of the nanoparticle and the uncertainty is estimated according to the error propagation formula. The laser power density I_{las} irradiated on the nanoparticles is an estimated value based on the laser power and the spot size. The parameters $\bar{v}$, γ, and a_c are taken from the literature [42,43]. The parameters ΔE and C, which are used to calculate the internal temperature of the levitated nanoparticle, are derived from the fitted calibration data. These parameters are summarized in Table II.

APPENDIX E: PARTICLE MOTION

As shown in Fig. 9, for temperature coupling constant measured in the z axis, there are similar results to the x and y axes. The temperature coupling constant K for the z axis is 0.32(5).

In Fig. 10, the internal temperature of the levitated nanoparticles before escaping from the optical trap shows a significant change. Although the air pressure, the rate of heating up, and the maximum temperature that these nanoparticles can reach before escaping from optical traps are different, they are all the same in that the internal temperature undergoes a slow increase process. This also suggests that the effect of the 976-nm laser on the nanoparticles is to heat the nanoparticles rather than to change the optical trap leading to the escape of the nanoparticles.

[1] A. Ashkin, Acceleration and Trapping of Particles by Radiation Pressure, Phys. Rev. Lett. **24**, 156 (1970).

[2] LSD Collaboration, G. Winstone, Z. Wang, S. Klomp, R. G. Felsted, A. Laeuger, C. Gupta, D. Grass, N. Aggarwal, J. Sprague, P. J. Pauzauskie, S. L. Larson, V. Kalogera, and A. A. Geraci, Optical Trapping of High-Aspect-Ratio NaYF Hexagonal Prisms for kHz-MHz Gravitational Wave Detectors, Phys. Rev. Lett. **129**, 053604 (2022).

[3] C. Gonzalez-Ballestero, M. Aspelmeyer, L. Novotny, R. Quidant, and O. Romero-Isart, Levitodynamics: Levitation and control of microscopic objects in vacuum, Science **374**, eabg3027 (2021).

[4] D. Lu, F. Gámez, and P. Haro-González, Temperature effects on optical trapping stability, Micromachines **12**, 954 (2021).

[5] F. Tebbenjohanns, M. L. Mattana, M. Rossi, M. Frimmer, and L. Novotny, Quantum control of a nanoparticle optically levitated in cryogenic free space, Nature (London) **595**, 378 (2021).

[6] J. Millen, T. Deesuwan, P. Barker, and J. Anders, Nanoscale temperature measurements using non-equilibrium Brownian dynamics of a levitated nanosphere, Nat. Nanotechnol. **9**, 425 (2014).

[7] E. Hebestreit, R. Reimann, M. Frimmer, and L. Novotny, Measuring the internal temperature of a levitated nanoparticle in high vacuum, Phys. Rev. A **97**, 043803 (2018).

[8] T. Agrenius, C. Gonzalez-Ballestero, P. Maurer, and O. Romero-Isart, Interaction between an Optically Levitated Nanoparticle and Its Thermal Image: Internal Thermometry via Displacement Sensing, Phys. Rev. Lett. **130**, 093601 (2023).

[9] T. M. Hoang, J. Ahn, J. Bang, and T. Li, Electron spin control of optically levitated nanodiamonds in vacuum, Nat. Commun. **7**, 12250 (2016).

[10] T. Delord, L. Nicolas, M. Bodini, and G. Hétet, Diamonds levitating in a Paul trap under vacuum: Measurements of laser-induced heating via NV center thermometry, Appl. Phys. Lett. **111**, 013101 (2017).

[11] F. Rivière, T. de Guillebon, L. Maumet, G. Hétet, M. Schmidt, J.-S. Lauret, and L. Rondin, Thermometry of an optically levitated nanodiamond, AVS Quantum Sci. **4**, 030801 (2022).

[12] A. T. M. A. Rahman and P. F. Barker, Laser refrigeration, alignment and rotation of levitated Yb^{3+}:YLF nanocrystals, Nat. Photonics **11**, 634 (2017).

[13] C. D. S. Brites, S. Balabhadra, and L. D. Carlos, Lanthanide-based thermometers: At the cutting-edge of luminescence thermometry, Adv. Opt. Mater. **7**, 1801239 (2019).

[14] D. Jaque and F. Vetrone, Luminescence nanothermometry, Nanoscale **4**, 4301 (2012).

[15] M. Suta and A. Meijerink, A theoretical framework for ratiometric single ion luminescent thermometers—Thermodynamic and kinetic guidelines for optimized performance, Adv. Theory Simul. **3**, 2000176 (2020).

[16] B. Zhang, X. Guo, Z. Zhang, Z. Fu, and H. Zheng, Luminescence thermometry with rare earth doped nanoparticles: Status and challenges, J. Lumin. **250**, 119110 (2022).

[17] F. Wang, Y. Han, C. S. Lim, Y. Lu, J. Wang, J. Xu, H. Chen, C. Zhang, M. Hong, and X. Liu, Simultaneous phase and size control of upconversion nanocrystals through lanthanide doping, Nature (London) **463**, 1061 (2010).

[18] P. Haro-González, B. del Rosal, L. M. Maestro, E. M. Rodríguez, R. Naccache, J. A. Capobianco, K. Dholakia, J. G. Solé, and D. Jaque, Optical trapping of $NaYF_4$:Er^{3+}, Yb^{3+} upconverting fluorescent nanoparticles, Nanoscale **5**, 12192 (2013).

[19] G. Nalupurackal, G. Murugan, M. Lokesh, R. Vaippully, A. Chauhan, B. R. K. Nanda, C. Sudakar, H. C. Kotamarthi, P. Datta, P. Sinha Mahapatra, A. Jannasch, E. Schäffer, S. Jayaraman, and B. Roy, Simultaneous optical trapping and electromagnetic micromanipulation of ferromagnetically doped $NaYF_4$ microparticles, ACS Appl. Opt. Mater. **1**, 615 (2023).

[20] M. Haase and H. Schäfer, Upconverting nanoparticles, Angew. Chem., Int. Ed. **50**, 5808 (2011).

[21] D. R. Luntz-Martin, D. R. Luntz-Martin, R. G. Felsted, S. Dadras, S. Dadras, P. J. Pauzauskie, P. J. Pauzauskie, A. N. Vamivakas, A. N. Vamivakas, A. N. Vamivakas, and A. N. Vamivakas, Laser refrigeration of optically levitated sodium yttrium fluoride nanocrystals, Opt. Lett. **46**, 3797 (2021).

[22] J. Li, Z. Chen, Y. Liu, P. S. Kollipara, Y. Feng, Z. Zhang, and Y. Zheng, Opto-refrigerative tweezers, Sci. Adv. **7**, eabh1101 (2021).

[23] A. T. M. A. Rahman, A. C. Frangeskou, P. F. Barker, and G. W. Morley, An analytical model for the detection of levitated nanoparticles in optomechanics, Rev. Sci. Instrum. **89**, 023109 (2018).

[24] E. Hebestreit, M. Frimmer, R. Reimann, C. Dellago, F. Ricci, and L. Novotny, Calibration and energy measurement of optically levitated nanoparticle sensors, Rev. Sci. Instrum. **89**, 033111 (2018).

[25] J. Gieseler, B. Deutsch, R. Quidant, and L. Novotny, Subkelvin Parametric Feedback Cooling of a Laser-Trapped Nanoparticle, Phys. Rev. Lett. **109**, 103603 (2012).

[26] J. Gieseler, L. Novotny, and R. Quidant, Thermal nonlinearities in a nanomechanical oscillator, Nat. Phys. **9**, 806 (2013).

[27] Z. H. Li, D. Hudry, R. Heid, A. H. Said, M. D. Le, R. Popescu, D. Gerthsen, M. Merz, K. W. Krämer, D. Busko, I. A. Howard, B. S. Richards, and F. Weber, Phonon density of states in lanthanide-based nanocrystals, Phys. Rev. B **102**, 165409 (2020).

[28] G. Sui, B. Chen, X. Zhang, X. Li, J. Zhang, S. Xu, J. Sun, Y. Cao, X. Wang, Y. Zhang, Y. Zhang, and X. Zhang, Radiative transition properties of Yb^{3+} in Er^{3+}/Yb^{3+} co-doped $NaYF_4$ phosphor, J. Alloys Compd. **834**, 155242 (2020).

[29] J. F. Suyver, J. Grimm, K. W. Krämer, and H. U. Güdel, Highly efficient near-infrared to visible up-conversion process in $NaYF_4$:Er^{3+}, Yb^{3+}, J. Lumin. **114**, 53 (2005).

[30] J.-C. Boyer, L. A. Cuccia, and J. A. Capobianco, Synthesis of Colloidal Upconverting $NaYF_4$: Er^{3+}/Yb^{3+} and Tm^{3+}/Yb^{3+} Monodisperse Nanocrystals, Nano Lett. **7**, 847 (2007).

[31] A. D. Pickel, A. Teitelboim, E. M. Chan, N. J. Borys, P. J. Schuck, and C. Dames, Apparent self-heating of individual upconverting nanoparticle thermometers, Nat. Commun. **9**, 4907 (2018).

[32] X. Xia, A. Volpi, J. Y. D. Roh, M. C. De Siena, D. R. Gamelin, M. P. Hehlen, and P. J. Pauzauskie, The impact of $^2H_{9/2} \rightarrow {}^4I_{13/2}$ emission from Er^{3+} ions on ratiometric optical temperature sensing with Yb^{3+}/Er^{3+} co-doped upconversion materials, J. Lumin. **236**, 118006 (2021).

[33] S. Balabhadra, M. L. Debasu, C. D. S. Brites, R. A. S. Ferreira, and L. D. Carlos, Upconverting nanoparticles working as primary thermometers in different media, J. Phys. Chem. C **121**, 13962 (2017).

[34] A. C. Frangeskou, A. T. M. A. Rahman, L. Gines, S. Mandal, O. A. Williams, P. F. Barker, and G. W. Morley, Pure nanodiamonds for levitated optomechanics in vacuum, New J. Phys. **20**, 043016 (2018).

[35] L. M. Wiesholler, F. Frenzel, B. Grauel, C. Würth, U. Resch-Genger, and T. Hirsch, Yb,Nd,Er-doped upconversion nanoparticles: 980 nm versus 808 nm excitation, Nanoscale **11**, 13440 (2019).

[36] F. Rivière, T. de Guillebon, D. Raynal, M. Schmidt, J.-S. Lauret, J.-F. Roch, and L. Rondin, Hot Brownian motion of optically levitated nanodiamonds, ACS Photonics **9**, 420 (2022).

[37] A. T. M. A. Rahman, A. C. Frangeskou, M. S. Kim, S. Bose, G. W. Morley, and P. F. Barker, Burning and graphitization of optically levitated nanodiamonds in vacuum, Sci. Rep. **6**, 21633 (2016).

[38] Y.-L. Pan, S. C. Hill, and M. Coleman, Photophoretic trapping of absorbing particles in air and measurement of their single-particle Raman spectra, Opt. Express **20**, 5325 (2012).

[39] R. Kitamura, L. Pilon, and M. Jonasz, Optical constants of silica glass from extreme ultraviolet to far infrared at near room temperature, Appl. Opt. **46**, 8118 (2007).

[40] Y. Zheng, L.-M. Zhou, Y. Dong, C.-W. Qiu, X.-D. Chen, G.-C. Guo, and F.-W. Sun, Robust Optical-Levitation-Based Metrology of Nanoparticle's Position and Mass, Phys. Rev. Lett. **124**, 223603 (2020).

[41] J. D. Kilbane, E. M. Chan, C. Monachon, N. J. Borys, E. S. Levy, A. D. Pickel, J. J. Urban, P. J. Schuck, and C. Dames, Far-field optical nanothermometry using individual sub-50 nm upconverting nanoparticles, Nanoscale **8**, 11611 (2016).

[42] W. Barnes, R. Laming, E. Tarbox, and P. Morkel, Absorption and emission cross section of Er/sup 3+/ doped silica fibers, IEEE J. Quantum Electron. **27**, 1004 (1991).

[43] G. Nemova, Laser cooling and trapping of rare-earth-doped particles, Appl. Sci. **12**, 3777 (2022).

[44] L. E. Mackenzie, J. A. Goode, A. Vakurov, P. P. Nampi, S. Saha, G. Jose, and P. A. Millner, The theoretical molecular weight of $NaYF_4$:RE upconversion nanoparticles, Sci. Rep. **8**, 1106 (2018).

[45] E. Mobini, M. Peysokhan, B. Abaie, M. P. Hehlen, and A. Mafi, Spectroscopic Investigation of Yb-Doped Silica Glass for Solid-State Optical Refrigeration, Phys. Rev. Appl. **11**, 014066 (2019).

[46] C. Homann, L. Krukewitt, F. Frenzel, B. Grauel, C. Würth, U. Resch-Genger, and M. Haase, $NaYF_4$:Yb,Er/$NaYF_4$ core/shell nanocrystals with high upconversion luminescence quantum yield, Angew. Chem., Int. Ed. **57**, 8765 (2018).